

Features of Liquid–Phase Epitaxy of $(\text{InSb})_{1-z}(\text{Sn}_2)_z$ Solid Solutions of Molecular Substitution on GaAs and GaP Substrates

Shukrullo Usmonov

Laboratory Growth of Semiconductor Crystals
Physical-Technical Institute
Tashkent, Uzbekistan
sh_usmonov@rambler.ru

Umida Asatova

Department of Physics
Urgench State University
Urgench, Uzbekistan
umida72@rambler.ru

Abduhakim Akhmedov

Department of Physics and Chemistry
Tashkent Institute of Irrigation and Agriculture
Mechanization Engineers
Tashkent, Uzbekistan
abdumirxakimaxmedov@gmail.com

Abstract — By the method of liquid-phase epitaxy, narrow-gap layers of solid solutions of indium antimonide molecular substitution were grown from a limited volume of indium solution - melt. The layers were grown on GaAs (100) and GaP (111) substrates.

It is shown that the binary compound of indium antimonide in an indium solution at temperatures of 350–220°C does not dissociate into individual In and Sb atoms, but is mainly in the form of InSb molecules. The photosensitivity of $n\text{GaAs}-p(\text{InSb})_{1-z}(\text{Sn}_2)_z$ and $n\text{GaP}-p(\text{InSb})_{1-z}(\text{Sn}_2)_z$ structures have been studied.

An anomalous temperature dependence of the current-voltage characteristic of the $n\text{GaP}-p(\text{InSb})_{1-z}(\text{Sn}_2)_z$ structure was found. The results are explained on the basis of a model that takes into account the possibility of the formation of defects and defect-impurity complexes of the “vacancy + recombination impurity center” type with increasing temperature.

Keywords— liquid-phase epitaxy, solubility in liquid metals, InSb, photosensitivity, narrow-gap solid solution

I. INTRODUCTION

One of the actual directions of development in the field of semiconductor materials science and optoelectronic instrumentation in world practice is the production and study of thin narrow-gap epitaxial films of solid solutions (SS) of elementary semiconductors and III–V binary compounds. Of particular importance among them are semiconductor materials with a fundamental absorption region corresponding to the near (with a wavelength of 1.6–5 μm) and medium (with a wavelength of 8–11 μm) infrared (IR) range of the radiation spectrum. Based on the III–V antimonide compound, $\text{InAs}_{1-z}\text{Sb}_z$ SS, and $\text{InAsSbP}/\text{InAsSb}$ heterostructures, LEDs [1–5] and IR photodetectors [6–14] operating in the wavelength range of 1.6–5 μm at room temperature have been created. These instruments are important for monitoring concentrations of a number of pollutants and toxic gases, as well as for medical diagnostics. Fundamental absorption bands

of industrial substances such as H_2O , CO_2 , CO , NO_2 , NH_3 , HF , H_2S , CH_4 , etc. lie in the wavelength range of 1.6–5 μm . IR emitters based on lead (IV–VI) salts [15], as well as on narrow-gap HgCdTe semiconductors [16], have low thermal conductivity and significant metallurgical instability, which makes them less suitable for use in industrial conditions than solid solutions of III–V. It is known that the 3–5 and 8–13 μm bands cover the atmospheric windows [17], where the atmospheric attenuation is relatively small. Therefore, the 3–5 μm band is used in practice to detect hot objects, such as vehicle and fighter aircraft engine exhausts [18, 19], while the 7.5–10.6 μm band is used in medical diagnostics as well as in various diagnostic measurements at room ambient temperatures [20–22]. Compounds of III–V antimonides and their solid solutions are promising materials for the development of such devices.

In this work the physical and technological features of growing $(\text{InSb})_{1-z}(\text{Sn}_2)_z$ solid solutions of molecular substitution on GaAs and GaP substrates were investigated. Some structural, electrical and photoelectric properties of structures based on this type solutions were also investigated.

II. METHODOLOGY

$(\text{InSb})_{1-z}(\text{Sn}_2)_z$ solid solutions were grown by liquid-phase epitaxy (LPE) from a limited volume of an indium solution-melt in a hydrogen atmosphere on a process plant with a vertically located quartz reactor [23]. Horizontally located substrates, in the graphite cassette of the reactor, were fixed, separated from each other by graphite supports. The melt solution was poured into the space between the substrates, the thickness of the solution-melt was determined by the distance between the substrates. The process of growth of epitaxial layers was carried out with varying component composition of the solution-melt (In–InSb–Sn), the thickness of the solution-melt in the range from 0.5 to 2.5 mm, the onset of the

crystallization temperature in the range from 300 to 400°C, the cooling rate of the solution-melt in within 0.5 to 2 °C/min. Polished GaAs (100) and GaP (111) wafers were used as substrates. The GaAs wafers had a diameter of 2 cm and, a thickness of 400 μm, *n*-type conductivity with a charge carrier concentration of $5 \cdot 10^{17} \text{ cm}^{-3}$. Gallium phosphide washers had a diameter of 2 cm, and a thickness of 350 μm, *n*-type conductivity with a charge carrier concentration of $6 \cdot 10^{17} \text{ cm}^{-3}$.

The chemical composition of the surface and cleavage of the epitaxial layer was determined using a "Jeol" JSM5910 LV-Japan X-ray microanalyzer.

Experimental studies of the dependence of the photosensitivity of *p-n* structures fabricated on the basis of the grown epitaxial layers on the photon energy were performed using an IKS-21 infrared spectrometer. The type of conductivity of the epitaxial layers was determined by the thermal probe method.

III. PROPOSED STRUCTURE AND PROPERTIES OF MATERIALS

The crystal structure of InSb has a cubic syngony of the zinc blende type, with a crystal lattice constant of 0.648 nm. Gray tin (α -Sn) also forms cubic crystals, with a crystal lattice constant of 0.646 nm, with a diamond-like structure. The sum of the valences of the InSb ($z_{\text{In}} + z_{\text{Sb}} = 3 + 5 = 8$) and Sn₂ ($z_{\text{Sn}} + z_{\text{Sn}} = 4 + 4 = 8$) atoms, as well as the sum of the covalent radii – InSb ($r_{\text{In}} + r_{\text{Sb}} = 2.80 \text{ \AA}$) and Sn₂ ($r_{\text{Sn}} + r_{\text{Sn}} = 2.80 \text{ \AA}$) are equal [24]. Therefore, they are promising pairs that form substitutional SSs of the (InSb)_{1-*z*}(Sn₂)_{*z*} type.

Fig. 1 shows the covalent bonds of the tetrahedral lattice of this SS. Since, there are also bonds of the Sn-Sb and In-Sn type in the tetrahedral lattice, in addition to the main covalent bonds of the SS components – Sn-Sn and In-Sb, the occurrence of an insignificant elastic deformation of a growth character is possible because of these bonds and due to the hybridization of the electron shells of neighboring atoms of the crystal lattice. However, the energy of elastic distortions in the crystal lattice, arising due to such deformations, will be insignificant, and the substitutional SS of (InSb)_{1-*z*}(Sn₂)_{*z*} will have a stable phase.

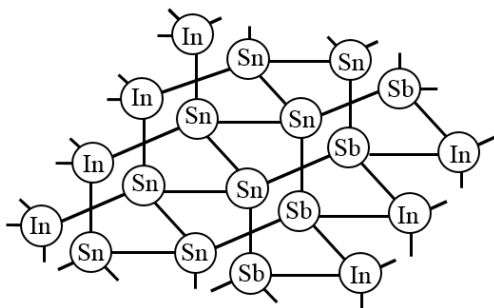


Fig. 1. Covalent bonds of the tetrahedral lattice of the solid solution (InSb)_{1-*z*}(Sn₂)_{*z*} of molecular substitution.

To grow the (InSb)_{1-*z*}(Sn₂)_{*z*} SS between InSb and Sn, it is necessary to create conditions for molecular substitution, i.e. molecules of indium antimonide (InSb) must be replaced by tin molecules (Sn₂). This requires that the SS components are in

the form of molecules in the liquid phase and have supersaturation at the crystallization onset temperature. These conditions can be implemented based on the model of A.S. Saidov [23] using a metallic solvent at temperatures lower than the melting point of the dissolved materials. We used In as a metallic solvent. The melting point of In under normal conditions is 156.6°C, while that of InSb and Sn is 527°C and 231.9°C, respectively. The solubility of InSb was determined by the weight loss method of InSb samples placed in liquid In and kept in it until the solution was saturated in the temperature range from 220 to 400°C. In this case, the influence of Sn on the solubility of InSb was considered. The composition of the solution-melt In-InSb-Sn was calculated on the basis of the literature data [25] and the results of preliminary experiments, taking into account the solubility of binary components.

When InSb is dissolved in In, at a temperature of 350°C, InSb molecules do not decompose into individual In and Sb atoms, but are in the form of an InSb molecule (Fig. 2a), since the temperature is insufficient to break the In-Sb covalent bond. The experimental results show that the solubility of InSb in In is low, and at a temperature of 350°C it is 7.4 mol.% (in the presence of the second component, tin, in the solution-melt).

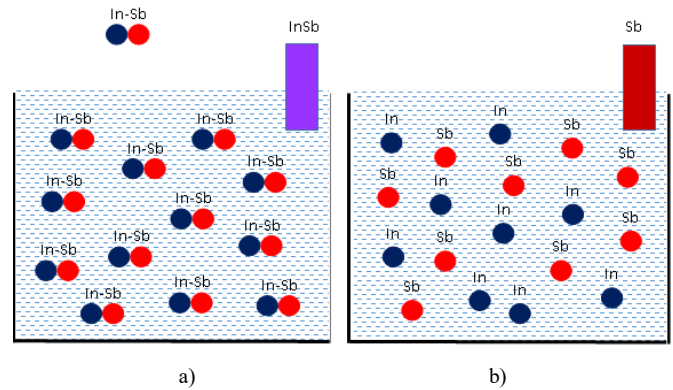


Fig. 2. Dissolution of indium antimonide in In: a) in the form of InSb molecules, b) in the form of individual In and Sb atoms

If the InSb molecules were separated into separate indium (In) and antimony (Sb) atoms (see Fig. 2b), then this would be equivalent to the dissolution of Sb in indium. At a temperature of 350°C, antimony in indium has a solubility of ~ 12 mol.% [25]. Then, respectively, the solubility of InSb in In at 350°C should have been 12 mol.%. However, this is not observed, the solubility of InSb in In is 7.4 mol.%. Therefore, it can be said that indium antimonide in an indium solution at a temperature of 350°C is mainly in the form of InSb molecules.

Epitaxial layers of SS (InSb)_{1-*z*}(Sn₂)_{*z*} with mirror-smooth surfaces and high crystalline perfection were grown at a distance between the upper and lower substrates of 1 mm, a crystallization temperature range of 325–220°C, and a cooling rate of the melt solution of 1 deg/min. The grown films had *p*-type conductivity [26–27].

The results of X-ray microanalysis and raster patterns along the cleavage and along the surface, made on the X-ray microanalyzer "Jeol" JSM5910 LV-Japan, showed that the epitaxial layers do not contain metal inclusions and the

distribution of components over the surface of the epitaxial layer is uniform, and in the volume of the solid solution $(\text{InSb})_{1-z}(\text{Sn}_2)_z$ varies within $0 \leq z \leq 0.05$. The entire surface of the substrate was covered with a continuous film firmly bonded to it.

Our previous study of the structure of epitaxial layers on the DRON-UM1 X-ray diffractometer using Cu anode radiation ($\lambda_\alpha = 1.5418 \text{ \AA}$, $\lambda_\beta = 1.3922 \text{ \AA}$) [27], showed that the layers have a single-crystal structure with the (100) orientation. The lattice parameter of the InSb epitaxial sublayer is 6.475 \AA , and that of the $(\text{InSb})_{1-z}(\text{Sn}_2)_z$ solid solution is 6.486 \AA .

IV. RESULTS AND DISCUSSIONS

A. Current transfer in the $n\text{GaP}-p(\text{InSb})_{1-z}(\text{Sn}_2)_z$ structure at different temperatures

To study the current transfer in $n-p$ structures based on $(\text{InSb})_{1-z}(\text{Sn}_2)_z$ SS, we fabricated $n\text{GaP}-p(\text{InSb})_{1-z}(\text{Sn}_2)_z$ ($0 \leq z \leq 0.05$) structures with continuous ohmic contacts on the side of the GaP substrate and quadrangular contacts with an area of 4 mm^2 on the side of the epitaxial layer. Typical current-voltage characteristics (CVC) of the structures under study, measured in the temperature range from 300 to 373 K, are shown in Figs. 3.

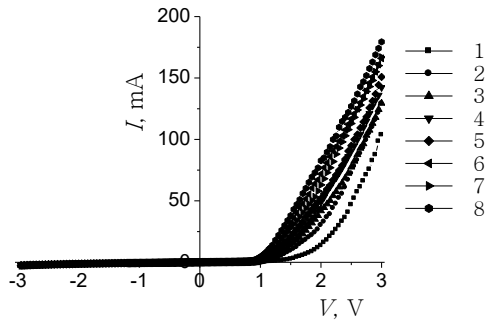


Fig. 3. Current-voltage characteristics of $n\text{GaP}-p(\text{InSb})_{1-z}(\text{Sn}_2)_z$ ($0 \leq z \leq 0.05$) structures at different temperatures: 1 – 300 K, 2 – 313 K, 3 – 323 K, 4 – 333 K, 5 – 343 K, 6 – 353 K, 7 – 363 K, 8 – 373 K.

Fig.3 shows that the structure exhibits rectifying properties throughout the measured temperature range. Up to 373 K, a sufficiently strong separation barrier remains in the structure under study. In the forward direction, the current-voltage characteristic at voltages above 1 V increases with increasing temperature, which indicates the significant role of thermal generation of electron-hole pairs in the narrow-gap semiconductor $(\text{InSb})_{1-z}(\text{Sn}_2)_z$ and their separation by an applied external field.

An analysis of the forward branch of the CVC shows that, in contrast to the high injection level ($V > 1 \text{ V}$), at low biases ($V < 0.8 \text{ V}$), an anomalous temperature dependence of the CVC is observed. The curve corresponding to 333 K lies lower than the curves corresponding to lower temperatures – 313 and 323 K. Only at 343 K the curves begin to rise with an increase in temperature. At 353 K, the maximum rise of the curves is observed, and with a further increase in temperature to 373 K,

their decline begins again. The same feature is also observed in the reverse branch of the CVC. However, in contrast to the direct branch, an anomalous temperature dependence is observed in the reverse branch over the entire measured voltage range; up to $V = 3 \text{ V}$.

Fig. 4. shows dependences of the current on the temperature of the studied structure for various voltage values in the direct (a) and reverse (b) branches of the CVC. Fig. 4 shows that at temperatures of 333 and 373 K, the current reaches its minimum values. To explain the observed phenomenon, one can use a model that takes into account the possibility of the formation of defects and defect-impurity complexes with an increase in temperature. [28].

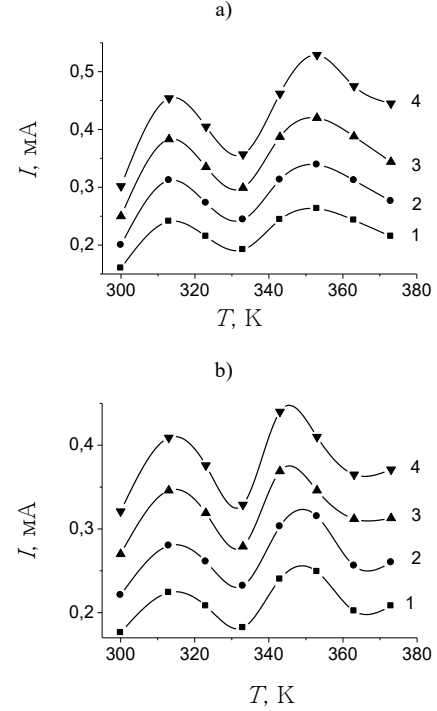


Fig. 4. Dependences of the current on temperature in the direct (a) and reverse (b) branches of the current-voltage characteristic of the $n\text{GaP}-p(\text{InSb})_{1-z}(\text{Sn}_2)_z$ ($0 \leq z \leq 0.05$) structure at constant voltage values: 1 - 0.4 V, 2 - 0.5 V, 3 - 0.6 V, 4 - 0.7 V.

The concentration of vacancies n_V in a semiconductor strongly depends on temperature [29]:

$$n_V = A \cdot \exp\left(-\frac{\Delta E_{Vac}}{kT}\right), \quad (1)$$

Where ΔE_{Vac} is the energy of vacancy creation. The birth of vacancies (n_V) and defect-impurity complexes (N_{RV}) of the “vacancy + recombination impurity center” type can be described by the equations:

$$\frac{dn_V}{dt} = B^* \cdot \exp\left(-\frac{\Delta E_{Vac}}{kT}\right) \cdot p - \frac{n_V - n_{V0}}{\tau_V}, \quad (2)$$

$$\frac{dN_{RV}}{dt} = \gamma \cdot N_R \cdot N_V - \frac{N_{RV} - N_{RV0}}{\tau_{RV}}, \quad (3)$$

where B^* is a constant depending on the electrical parameters of the material, n_{V0} и N_{RV0} are the initial concentrations of vacancies and defect-impurity complexes, respectively, N_{RV} is the concentration of defect-impurity complexes, τ_V and τ_{RV} are the lifetimes of vacancies and defect-impurity complexes, accordingly, p – is the concentration of free charge carriers, γ – is the coefficient describing the probability of the birth of defect-impurity complexes.

Under stationary conditions ($dn_V/dt = 0$, $dN_{RV}/dt = 0$) can be determined n_V and N_{RV} from (1) and (2):

$$n_V = n_{V0} + B^* \tau_V \cdot \exp\left(-\frac{\Delta E_{Vac}}{kT}\right) \cdot p, \quad (4)$$

$$N_{RV} = N_{RV0} + \gamma \tau_{RV} n_{V0} N_R + B^* \gamma \tau_{RV} \tau_V N_R \exp\left(-\frac{\Delta E_{Vac}}{kT}\right) p. \quad (5)$$

Under these conditions, the recombination rate (U) of free charge carriers will be determined by the concentration of efficiently operating recombination centers ($N_{R,eff}$) $N_{R,eff} = N_R - N_{RV}$ and will take the form:

$$U = (N_R - N_{RV}) \cdot \frac{c_n c_p (pn - n_i^2)}{c_n (n + n_1) + c_p (p + p_1)}, \quad (6)$$

Where c_n and c_p are the coefficients of electron and hole capture by recombination centers, respectively, n and p are the concentrations of nonequilibrium electrons and holes, respectively, n_i is the concentration of equilibrium carriers in the intrinsic semiconductor, n_1 and p_1 are the Shockley-Read statistical factors.

It can be seen from (6) that, in contrast to classical statistics, the recombination rate may decrease with an increase in the excitation level. The critical point at which it begins can be determined by equating the derivative dU/dt to zero, $N_R - 2\chi \cdot p_{cr} = 0$, where, $\chi = AN_R \tau_V \tau_{RV} \exp(-\Delta E_{Vac}/kT)$, $p_{cr} = N_R/2\chi$ is the concentration of free charge carriers at which the decrease in the $U(p)$ dependence begins. This explains well the drop in current at a certain temperature. Thus, at this concentration, the rate of recombination of charge carriers stop increasing linearly with temperature and, accordingly, the lifetime of nonequilibrium charge carriers $\tau = p/U$ will no longer be a constant value, but will increase with the level of excitation. Accordingly, the diffusion length of nonequilibrium charge carriers $L = \sqrt{D\tau}$ will also increase with an increase in the excitation level. Therefore, even in the simplest case, when the current through the n - p junction is determined by the expression:

$$I = 2q \frac{Dp}{L} p(0) \quad (7)$$

its decrease with an increase in temperature is possible due to an increase in the value of L . This well explains the decay of the $I(V)$ curves recorded by us with temperature. However, with a further increase in temperature, the direct recombination of charge carriers through vacancy levels should also begin to

play a role. Then $U(p)$ will again increase with the excitation level, which well explains the observed increase in current on the $I(V)$ curves in the temperature range 333–353 K.

B. Photoelectric characteristics of $(InSb)_{1-z}(Sn_2)_z$ ($0 \leq z \leq 0.05$) solid solution layers and heterostructures based on them.

The photosensitivity of the studied structures was estimated on the basis of the short-circuit photocurrent of heterostructures at different wavelengths of electromagnetic radiation. The photocurrent was normalized to a single photon in the entire studied range of radiation wavelengths.

The measurement results are shown in fig. 5. It can be seen that the photosensitivity of both structures are identical and cover a wide wavelength range of 1.0–5.3 μm with a maximum at 1.65 μm . However, other things being equal, the photoresponse in the $nGaP$ - $p(InSb)_{1-z}(Sn_2)_z$ structure is two times greater than in the case of $nGaAs$ - $p(InSb)_{1-z}(Sn_2)_z$. This is apparently due to the difference in potential barriers formed in the electron-hole transition between the $nGaP$ and $nGaAs$ substrate and the p - $(InSb)_{1-z}(Sn_2)_z$ epitaxial layer. This barrier is a separating barrier for nonequilibrium photogenerated charge carriers. Due to the difference in the band gap between GaP and GaAs, the potential barrier formed in the $nGaP$ - $p(InSb)_{1-z}(Sn_2)_z$ heterostructure is much larger than in the case of $nGaAs$ - $p(InSb)_{1-z}(Sn_2)_z$. The photosensitivity of the studied structures in the long-wavelength spectral range is limited at a wavelength of 5.3 μm . The insufficiency of completeness of absorption of the narrow-gap layer of SS $(InSb)_{1-z}(Sn_2)_z$ ($0 \leq z \leq 0.05$) in the long-wavelength region of the emission spectrum is due to the small thickness of the upper sublayer of the solid solution enriched with tin. The decrease in photosensitivity in the short-wavelength region is due to the depth of the separating potential barrier of the n - p junction, which in this case is $\sim 14 \mu\text{m}$, which is more than the diffusion length of minority charge carriers – $L_n \approx 2.9 \mu\text{m}$. Photocarriers generated by photons with a wavelength of $\lambda < 1 \mu\text{m}$ do not reach the separating barrier of the p - n junction and do not contribute to the photocurrent, consequently.

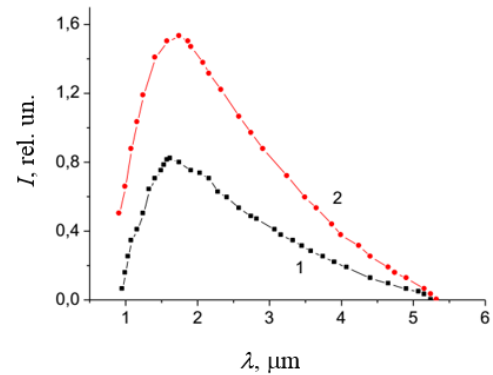


Fig. 5. Dependences of photosensitivity $nGaAs$ - $p(InSb)_{1-z}(Sn_2)_z$ ($0 \leq z \leq 0.05$) (curve 1) and $nGaP$ - $p(InSb)_{1-z}(Sn_2)_z$ ($0 \leq z \leq 0.05$) (curve 2) of heterostructures on the wavelength of electromagnetic radiation

V. CONCLUSIONS

Thus, based on the elemental semiconductor tin and the binary compound InSb, under certain technological conditions, a solid solution of molecular substitution $(\text{InSb})_{1-z}(\text{Sn}_2)_z$ ($0 \leq z \leq 0.05$) can be obtained from the limited volume of an indium solution–melt. The epitaxial layers have a perfect single–crystal structure. Under the influence of tin atoms, the resulting solid solution has a narrow band gap $E_{g,ss} = 0.11$ eV. Such solid solutions can be used to develop optoelectronic devices operating in the near–IR region of the radiation spectrum.

ACKNOWLEDGMENT

The authors gratefully acknowledge Prof. Dr. Amin Saidov, Chief Researcher at the Physical–technical Institute of the Academy of Sciences of the Republic of Uzbekistan, for valuable advice and discussion of the experimental results.

REFERENCES

- [1] S.S. Kizhayev, N.V. Zotova, S.S. Molchanov, B.V. Pushnyi, Yu.P. Yakovlev, “Powerful InAsSbP/InAsSb light emitting diodes grown by MOVPE”, *Journal of Crystal Growth*, vol. 248, pp. 296–300, 2003.
- [2] N. V. Zotova, N. D. Il’inskaya, S. A. Karandashev, B. A. Matveev, M. A. Remennyi and N. M. Stus’, “Flip-Chip LEDs with Deep Mesa Emitting at 4.2 μm ”, *Semiconductors*, vol. 40, no. 6, pp. 697–703, 2006.
- [3] V. V. Romanova, I. A. Belykha, E. V. Ivanova, P. A. Alekseeva, N. D. Il’inskayaa and Yu. P. Yakovleva, “Light-Emitting Diodes Based on an Asymmetrical InAs/InAsSb/InAsSbP Double Heterostructure for CO_2 ($\lambda = 4.3 \mu\text{m}$) and CO ($\lambda = 4.7 \mu\text{m}$) Detection”, *Semiconductors*, vol. 53, no. 6, pp. 822–827, 2019.
- [4] Maya Mikhailova, Nikolay Stoyanov, Igor Andreev, Bizhigit Zhurtanov, Sergei Kizhaev, Ekaterina Kunitsyna, Khafiz Salikhov, Yury Yakovlev, “Optoelectronic sensors on GaSb- and InAs- based heterostructures for ecological monitoring and medical diagnostics”, *Proc. SPIE 6585, Optical Sensing Technology and Applications*, 658526 (16 May 2007); Event: International Congress on Optics and Optoelectronics, Prague, Czech Republic, 2007.
- [5] Maya Mikhailova, Nikolay Stoyanov, Igor Andreev, Bizhigit Zhurtanov, Sergei Kizhaev, Ekaterina Kunitsyna, Khafiz Salikhov, Yury Yakovlev. “Optoelectronic sensors on GaSb- and InAs-based heterostructures for ecological monitoring and medical diagnostics”, *Proceedings Volume 6585, Optical Sensing Technology and Applications*; 658526; Event: International Congress on Optics and Optoelectronics, Prague, Czech Republic, 2007.
- [6] S. Maimon and G. W. Wicks, “nBn detector, an infrared detector with reduced dark current and higher operating temperature”, *Applied Physics Letters*, vol. 89, 151109, 2006.
- [7] A. Haddadi, R. Chevallier, G. Chen, A. M. Hoang and M. Razeghia, “Bias-selectable dual-band mid-/long-wavelength infrared photodetectors based on InAs/InAs $_{1-x}$ Sb $_x$ type-II superlattices”, *Appl. Phys. Lett.*, vol. 106, 011104, 2015.
- [8] Philip Klipstein, “XB<i>n</i> barrier photodetectors for high sensitivity and high operating temperature infrared sensors”, *Proc. SPIE 6940, Infrared Technology and Applications XXXIV*, 69402U, 2008.
- [9] Neil Baril, I. Alexander Brown, Patrick Maloney, Meimei Tidrow, Dmitri Lubyshev, Yueming Qui, Joel M. Fastenau, Amy W. K. Liu and Sumith Bandara, “Bulk InAs $_x$ Sb $_{1-x}$ nBn photodetectors with greater than 5 μm cutoff on GaSb”, *Appl. Phys. Lett.*, vol. 109, 122104, 2016.
- [10] P. Craig, A. R. J. Marshall, Z.-B. Tian, S. Krishna and A. Krier, “Mid-infrared InAs $_{0.79}$ Sb $_{0.21}$ -based nBn photodetectors with Al $_{0.9}$ Ga $_{0.2}$ As $_{0.1}$ Sb $_{0.9}$ barrier layers, and comparisons with InAs $_{0.87}$ Sb $_{0.13}$ p-i-n diodes, both grown on GaAs using interfacial misfit arrays”, *Appl. Phys. Lett.*, vol. 103, 253502, 2013.
- [11] Neil Baril, Alexander Brown, Daniel Zuo, Meimei Tidrow, Dmitri Loubychev, Joel M. Fastenau, Amy W. K. Liu, Sumith Bandara, “MWIR barrier infrared detectors with greater than 5 μm cutoff using bulk InAsSb grown on GaSb substrates”, *Proc. SPIE 10177, Infrared Technology and Applications XLIII*, 101771L, 2017.
- [12] D. Zuo, R. Liu, D. Wasserman, J. Mabon, Z.-Y. He, S. Liu, Y.-H. Zhang, E. A. Kadlec, B. V. Olson and E. A. Shaner, “Direct minority carrier transport characterization of InAs/InAsSb superlattice nBn photodetectors”, *Appl. Phys. Lett.*, vol. 106, 071107, 2015.
- [13] X.-M. Shen, Z.-Y. He, S. Liu, Z.-Y. Lin, Y.-H. Zhang, D. J. Smith and M. R. McCartney, “An indirect method of studying band alignments in nBn photodetectors using off-axis electron holography”, *Appl. Phys. Lett.*, vol. 107, 122109, 2015.
- [14] V. Olson, E. A. Shaner, J. K. Kim, J. F. Klem, S. D. Hawkins, L. M. Murray, J. P. Prineas, M. E. Flatt_e and T. F. Boggess, “Time-resolved optical measurements of minority carrier recombination in a mid-wave infrared InAsSb alloy and InAs/InAsSb superlattice”, *Appl. Phys. Lett.*, vol. 101, 092109, 2012.
- [15] Z. Feit, D. Kostyk, R.J. Woods, P. Mak, “Single-mode molecular beam epitaxy grown PbEuSeTe/PbTe buried-heterostructure diode lasers for CO_2 high-resolution spectroscopy” *Appl. Phys. Lett.*, Vol. 58, no. 4, pp. 343-345, 1991.
- [16] E. Hadji, J. Bleuse, N. Magnea, J. L. Pautrat, “3.2 μm infrared resonant cavity light emitting diode”, *Applied Physics Letters*, vol. 67, no. 18, pp.2591-2593, 1995.
- [17] H. A. Gebbie, W. R. Harding, C. Hilsum, A. W. Pryce and V. Roberts, “Atmospheric transmission in the 1 to 14 μm region”, *Proceedings of the Royal Society (London) Series A*, vol. 206, no. 1084, pp. 87–10, 1951.
- [18] G. A. Rao and S. P. Mahulikar, “Integrated review of stealth technology and its role in airpower”, *The Aeronautical Journal*, vol. 106, no. 1066, pp. 629–641, 2002.
- [19] S. P. Mahulikar, H. R. Sonawane and G. A. Rao, “Infrared signature studies of aerospace vehicles”, *Progress in Aerospace Sciences*, vol. 43, no. 7–8, pp. 218–245, 2007.
- [20] S. P. Mahulikar, G. A. Rao, H. R. Sonawane and H. S. S. Prasad, “Infrared Signature Studies of Aircraft and Helicopters”, *PIERS Proceedings*, Moscow, Russia, pp. 26-30, 2009.
- [21] E. Costard, Ph. Bois, “THALES long wave QWIP thermal imagers”, *Infrared Physics & Technology*, vol. 50, pp. 260–269, 2007.
- [22] D. Peric, B. Livada, M. Peric, S.Vujic, “Thermal imager range: Predictions, expectations, and reality”, *Sensors*, vol. 19, no. 15, p. 3313, 2019.
- [23] A. S. Saidov, Sh. N. Usmonov and D. V. Saparov, “Structural Studies of the Epitaxial Layer of a Substitutional Solid Solution $(\text{GaAs})_{1-x}(\text{ZnSe})_x$ with Nanocrystals”, *Advances in Materials Science and Engineering*, Article ID 3932195, 2019.
- [24] David R. Lide. *CRC Handbook of Chemistry and Physics*, 87th edition (National Institute of Standards and Technology) Copyright CRC Press LLC. 2007.
- [25] M. Hansen and K. Anderko, “Constitution of Binary Alloys” (McGraw_Hill, New York, 1958; Metallurgiya, Moscow, 1962), vol. I & II, 1962.
- [26] A.S. Saidov, Sh.N.Usmonov, U.P. Asatova, “Thermoelectric Properties of n-Ge–p-(InSb) $_{1-x}$ (Sn $_2$) $_x$ Heterostructures”, *Applied Solar Energy*, vol. 46, no. 2, pp. 104–106, 2010.
- [27] A. S. Saidov, M. S. Saidov , S. N. Usmonov, U. P. Asatova, “Growth of (InSb) $_{1-x}$ (Sn $_2$) $_x$ films on GaAs substrates by liquid-phase epitaxy”, *Semiconductors*, vol. 44, no. 7, pp. 938-945, 2010.
- [28] A. Y. Leiderman, V. G. Stel’makh, M. Sadykov, “Recombination in semiconductors with deep impurities”, *Applied Solar Energy*, vol.44, no. 4, pp. 276-280, 2008.
- [29] V. I. Fistul, *Introduction to Semiconductor Physics*, Moscow, Higher school, p.352, 1984 (V. I. Fistul, Vvedenie v fiziku poluprovodnikov. Moskva, Vysshaja shkola, 352 s.).